Observation of Double Fano Interference in Metal-Insulator Block Arrays

Wenchen Yang
Hongyan Yang
Shuwen Xue
Ling Guo
Lizhen Zeng
Gongli Xiao

Observation of Double Fano Interference in Metal-Insulator Block Arrays

Wenchen Yang,[1] Hongyan Yang ®,[2,3] Shuwen Xue,[1] Ling Guo,[3] Lizhen Zeng,[4] and Gongli Xiao ®[1]

[1]Guangxi Key Laboratory of Precision Navigation Technology and Application, Guilin University of Electronic Technology, Guilin 541004, China
[2]Guangxi Key Laboratory of Automatic Detecting Technology and Instruments, Guilin University of Electronic Technology, Guilin 541004, China
[3]School of Electronic Engineering and Automation, Guilin University of Electronic Technology, Guilin 541004, China
[4]Graduate school, Guilin University of Electronic Technology, Guilin 541004, China

Abstract: The coexistence of double Fano interference originating from anti-phased and in-phased lattice resonances is observed in a novel plasmonic lattice array, which being consists of a horizontal double-stacked rectangular metal-insulator block. Based on a classic model analysis of coupled harmonic oscillators, the observed double Fano interference is revealed as a result of the interaction between a bright broad resonance and a dark narrow one as well as the coupling of narrow and broad spectral lines. This allows for active tuning of the double Fano resonance to a desired spectral position by a controlled size variation of the metal-insulator block arrays. After optimizing the parameters, they display two narrow absorbance peaks with high-quality factors of 84.92 and 214.1, respectively. This is because of the utmost enhancements of local electric fields in the gap between two opposing rectangular metal blocks. We expect that double Fano interference character may gain more significant potential applications in biomedical sensing.

Index Terms: Fano interference, metal-insulator block arrays, lattice resonances effect.

1. Introduction

Fano resonances have become an active topic of current research owing to their unusual optical properties. The visible and near-infrared spectral range has been successfully observed experimentally for a multitude of plasmonic nanostructures [1], [2]. To pattern nanoparticles in periodic arrays can have a profound impact on significant field enhancement over large volumes and, in particular, it can enable the excitation of otherwise dark modes to generate Fano resonances [3]–[8]. These more promising optical features may enable a diverse range of practical applications,

including optical filtering [9], sensing [10], [11], polarization selectors [12], lasers [13], and switching [14].

The original Fano resonance is based on the destructive and constructive interferences that occur at close energy positions [7]. Its Lorentzian line-shape gives away to a sharp change between a dip and a peak [15], [16]. Its forming mechanism is produced by the interference between a resonant dark mode and a flat continuum of radiative waves [17]. Moreover, in the lattice array, the electric field component of the incident light (E_{inc}) can induce dipoles moment in each nanoparticle [18]. It sometimes exhibits as in-plane dipoles and out-of-plane quardrupoles due to their different polarizability, leading to retarded electric fields (E_{dipole}) formed by the summing dipoles moment and E_{inc} coexist in the array [19], [20]. The coupling of two or more single nanoparticles and symmetry-breaking nanostructures has been extensively studied to enhance light-matter interactions, such as square-shaped metal-insulator-metal (MIM) nanopillars [20], closely packed nanoparticle clusters [21]–[24] and multifold nanorods [25]. Another striking interaction that a broad bright mode (in-phased lattice collective resonance, ILCR) and a narrow dark mode (anti-phased lattice collective resonance, ALCR) takes advantage of Fano interference between subradiant and superradiant plasmon resonances can be observed [23], [26]. This plasmonic mode hybridization is qualitatively similar to the electromagnetically induced transparency (EIT) phenomenon in atomic physics [27]. Their EIT-like spectra arise from a meaningful trapped mode in a large scattering cross-section [28,29]. And the typical formation is that plasmonic polarization of adjacent nanoparticles oppositely oscillates respecting each other, leading to destructive interference with the radiative far-fields [21], [26]. Two oscillators with different damping rates can describe the EIT-like interference and the original Fano resonance [16], and the dark mode is excited just due to their weakly coupling [7]. Thus, seeking new strategies to effect coupling mechanisms and exciting a dark plasmonic state are very active areas of nanoscience research. However, a detailed study for both the EIT-like interference and the original Fano resonance are excited in a nanostructure simultaneously has not been carried out to date since the dark mode is usually formed in a single pathway.

In this paper, for the first time to our knowledge, we theoretically verify the coexistence of double Fano interference in metal-insulator block arrays. We observe the characteristic suppression of the extinction associated with the double Fano resonances spectra. We further discuss the underlying physics of the observed double Fano resonances by employing a novel theoretical approach based on the model of coupled harmonic oscillators [16], [30]. The asymmetrical distribution of insulator blocks gives out a significant effect on exciting two different dark modes. The remarkably enhanced electric fields trapped in the middle insulator exhibit two narrow absorbance peaks with high-quality factors (Q = 84.92 and Q = 214.1). This analysis confirms that the observed double Fano resonances originate from the predominant excitation of the EIT-like interference and the original Fano resonance, and provide a useful insight into their tuning behavior. Importantly, by using this property for sensor analysis, the sensitivity and the figure of merit (FOM) can reach as high as 258.3 nm/RIU and 320 nm/RIU, 28.7 and 38.6, respectively. Their attractive benefits may find high potential applications in biological sensing.

2. Simulation Setup

The numerical simulations are carried out using a finite-difference time-domain (FDTD) technique in commercial FDTD software package from Lumerical Inc. In the simulation, perfectly matched layer (PML) boundary conditions are set in the top and bottom z planes. In contrast, periodic boundary conditions in x and y directions are applied to simulate an infinite area. The mesh unit of the MIMI structure is set to 2 nm to ensure the accuracy of the calculation. We take the rectangular metal blocks to be silver and take the rectangular insulator blocks to be silica with wavelength-dependent complex dielectric constants, n and k, tabulated in [31] and [32], respectively. And we adopt the polymer PU substrate with $n_1 = 1.52$ [6], unless otherwise specified, the superstrate is taken to be air ($n_2 = 1.0$). Fig. 1(a) illustrates the three-dimensional structure schematic of the rectangular MIMI block arrays in an asymmetric dielectric environment ($n_1 \neq n_2$). The widths of two opposite rectangular metal blocks are $w_1 = 40$ nm and $w_2 = 40$ nm, and the widths of two opposite
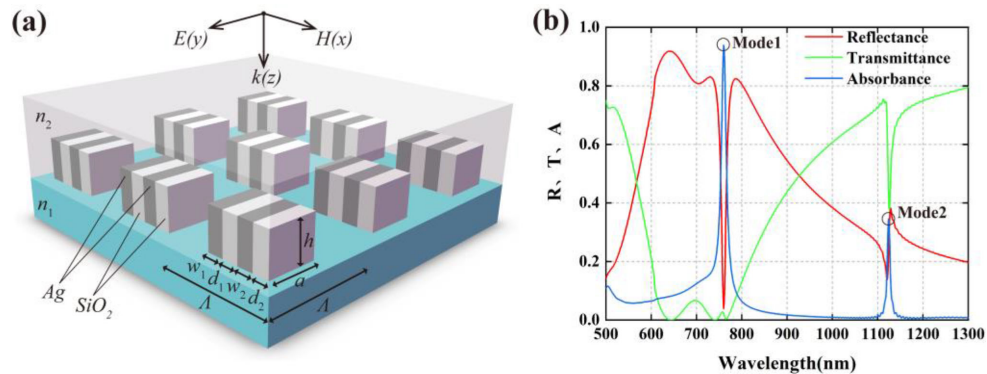
Fig. 1. (a) The schematic of rectangular MIMI block arrays in an asymmetric dielectric environment ($n_1 \neq n_2$). (b) Reflectance, transmittance, and absorbance spectra of the structure.

rectangular insulator blocks are $d_1 = 50$ nm and $d_2 = 50$ nm, respectively. Each rectangular block is $h = 180$ nm in height and $a = 230$ nm in length, and the array periods along both the x and y axes are equal to $\Lambda = 400$ nm. The rectangular MIMI block arrays are located on a substrate with refractive index n_1, which is covered by a sufficiently thick superstrate with refractive index n_2. A plane wave illuminates it under a normal incidence, and the polarization direction is parallel to y-axes.

It is profoundly challenging to fabricate the structure. To realize higher precision, we suggest first using electron-beam evaporation to deposit the silver onto the substrate. The next step is forming the periodic grooves with the width d_2 and d_1 along the y-direction by photolithography and etching. Then, the third step is depositing the silica and removing the photoresist. Finally, the MIMI structure can be obtained by the second photolithography and etching of redundant silver and silica after chemical mechanical polishing. Photolithographic alignment only has high accuracy requirements in the x-direction.

Fig. 1(b) shows the proposed structure exhibits a narrow dip, which is centered at $\lambda = 760$ nm existing within a broad reflectance peak in the Mode1 under normal incidence. Defined quality factor as $Q = \lambda/\Delta\lambda$, it correspondingly leads to a narrow peak with a full-with-half-maximum (FWHM) of $\Delta\lambda = 8.95$ nm and $Q = 84.92$ in absorbance. In the Mode2, the reflectance shows an asymmetry with a sharp change between a dip and a peak, which is the typical Fano response. And the resonance with a dip in transmittance also results in another narrow peak in absorbance with $\Delta\lambda = 5.25$ nm and higher $Q = 214.1$ at the wavelength of $\lambda = 1124$ nm.

3. Results and Discussion

3.1 Spectral Characteristics and Near-Fields Analysis

When the polarization direction is parallel to y-axes, the reflectance of rectangular block arrays is investigated both in symmetric MIM structure and asymmetric MIMI structure cases, and that is given out in Fig. 2(a). Mode2 cannot be directly excited in the symmetric MIM structure, whereas the asymmetric MIMI structure can effectively enhance the resonance role of Mode1. This indicates the coexistence of double Fano interference is attributed to the asymmetric distribution of rectangular silica blocks, and their different mechanisms are also shown in Fig. 2(b). The Mode1 exhibiting the spectral profile of the EIT-like interference, arises from a narrow dark mode destructive interferes with a broad bright mode. The Mode2 is the original Fano resonance, which builds from the interference between a nonradiative dark mode and a continuum of radiative waves spectrally and spatially overlapped [17].

To elucidate the difference of two fundamental Fano interferences. We simulate their optical near-fields distributions at the wavelengths of the broad reflectance peak ($\lambda_1 = 640$ nm), the
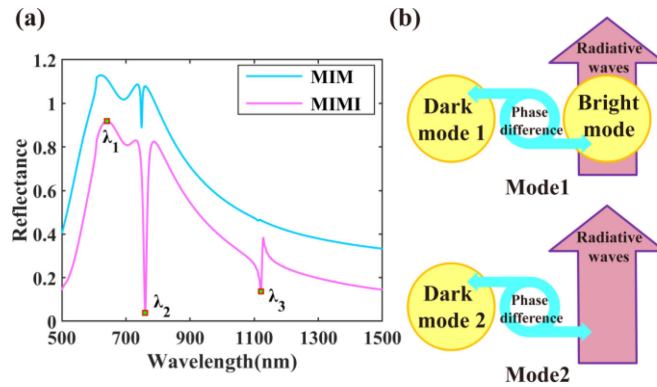
Fig. 2. (a) Reflectance spectra of the symmetric MIM and asymmetric MIMI two structures. (b) Mechanism of two different Fano interferences (reproduced from [ref. 17]).
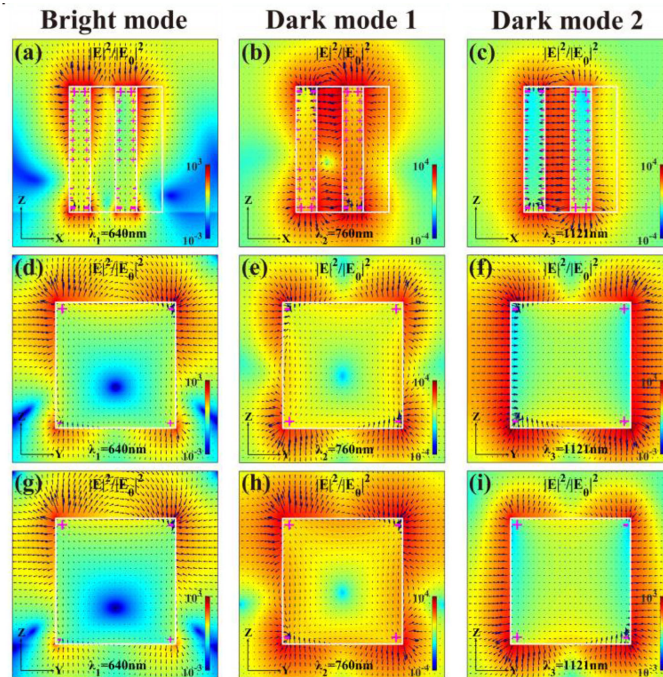

Fig. 3. Electric field intensity (in color) and vector (in arrows) maps of the cross section in x-z plane at $\lambda_1 = 640$ nm of the broad reflectance peak (left column), at $\lambda_2 = 760$ nm of the narrow reflectance dip (center column), and at $\lambda_3 = 1121$ nm of the asymmetric Fano line-shape dip (right column) of (a)–(c), and that of the left rectangular metal block in the y-z plane of (d)–(f), and that of the right rectangular metal block in y-z plane of (g)–(i).

reflectance dip ($\lambda_2 = 760$ nm), and the dip of Fano line-shape ($\lambda_3 = 1121$ nm), as shown in Fig. 3. At $\lambda_1 = 640$ nm, a robust in-plane dipole can be excited in the top ridge of the rectangular metal block, which further induces a weaker anti-phased in-plane dipole in the bottom metal ridge. All the dipoles have the same phase, which is the ILCR mode and manifests the collective lattice resonance of the constituent nanoparticle individuals in the array [34]. In the ILCR mode, all dipoles oscillate in-phase or anti-phase with the incident light. Thus, the retarded electric field E_{dipole} formed by them constructively interferes with the electric field E_{inc} of the incident light [20], [26]. It can be seen as a bright mode with the reflectance is effectively enhanced. Whereas at $\lambda_2 = 760$ nm,
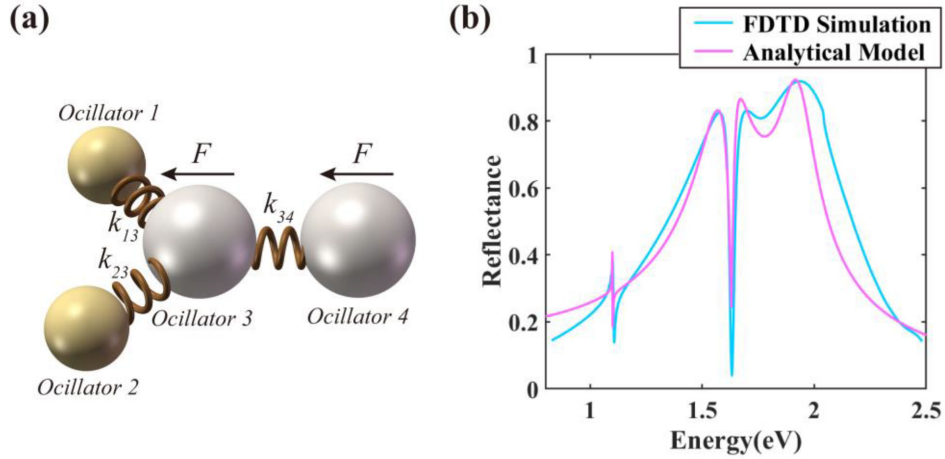
Fig. 4. (a) The diagram of coupled oscillators model. (b) The comparison of two reflectance spectra being calculated by the FDTD simulation and analytical model respectively.

two anti-phased out-of-plane quardrupoles are excited in the opposing rectangular metal blocks, respectively, resulting in an effective electric field trap, as shown in Fig. 3(b). It is the ALCR mode that manifests one of quardrupoles oscillates in-phase while the other oscillates anti-phase with the incident light [26]. The trapping electric fields have a destructive interference in the far-fields generating the elimination of scattering loss, which is the dark mode1 with the reflectance is significantly minimized. And at $\lambda_3 = 1121$ nm, the opposing rectangular metal blocks exhibit a pair of in-plane dipoles at tops and bottoms. Similarly, the electric fields are highly restricted in the metal edges and corners. As shown in Fig. 3(c), they are also anti-phased. They have effective light trapping and extreme field enhancement in the middle silica insulator, forming the dark mode2 with a similar effect on suppressing radiative far-fields.

3.2 The Model of Coupled Driven Oscillators

The ILCR mode exciting in-phased dipoles in rectangular metal blocks is directly induced by the E_{inc} along the y-axis. And these redistributing dipoles are toggled by the wavelength of the incident light. The asymmetric distribution of rectangular silica blocks further affects their inharmonious shift in the opposing rectangular metal blocks, which leads to the coupled ALCR mode exhibiting anti-phased quardrupoles and dipoles are indirectly excited. Driven oscillators can interpret the physical origin of the Mode1 and the Mode2 with unequal damping rates in different coupling regimes [16]. The scattering losses of the array can be viewed as two driven oscillators with more significant damping. In contrast, the dark mode1 and the dark mode2 are two weakly damped oscillators that couple to one of two damping oscillators, as shown in Fig. 4(a).

When two damping oscillators are driven strongly by the external force F with the driving frequency ω, the equations of motion of the four oscillators can be described as [30]:

$$\begin{cases} \ddot{x}_1(t) + \gamma_1 \dot{x}_1(t) + \omega_1^2 x_1(t) - k_{13} x_3(t) = 0 \\ \ddot{x}_2(t) + \gamma_2 \dot{x}_2(t) + \omega_2^2 x_2(t) - k_{23} x_3(t) = 0 \\ \ddot{x}_3(t) + \gamma_3 \dot{x}_3(t) + \omega_3^2 x_3(t) - k_{13} x_1(t) - k_{23} x_2(t) - k_{34} x_4(t) = F e^{i\omega t} \\ \ddot{x}_4(t) + \gamma_4 \dot{x}_4(t) + \omega_4^2 x_4(t) - k_{34} x_3(t) = F e^{i\omega t} \end{cases} , \tag{1}$$

where $x_i(t)$, ω_i and γ_i ($i = 1, 2, 3, 4$) are displacements, resonant frequencies, and damping coefficients of four oscillators. k_{13}, k_{23}, and k_{34} are the coupling constant between the oscillators. That we assume the displacements of the oscillators are harmonic is used for the convenience of

solving, such that,

$$x_1(t) = ae^{i\omega t}, \, x_2(t) = be^{i\omega t}, \, x_3(t) = ce^{i\omega t}, \, x_4(t) = de^{i\omega t}. \tag{2}$$

The amplitude of oscillator 3 and oscillator 4 can be written as

$$|c| = \left| \frac{\omega_4^2 - \omega^2 + i\omega\gamma_4 + k_{34}}{\left[\omega_3^2 - \omega^2 + i\omega\gamma_3 - k_{13}^2/(\omega_1^2 - \omega^2 + i\omega\gamma_1) - k_{23}^2/(\omega_2^2 - \omega^2 + i\omega\gamma_2)\right](\omega_4^2 - \omega^2 + i\omega\gamma_4) - k_{34}^2} F \right|, \tag{3}$$

$$|d| = \left| \frac{\omega_3^2 - \omega^2 + i\omega\gamma_3 - k_{13}^2/(\omega_1^2 - \omega^2 + i\omega\gamma_1) - k_{23}^2/(\omega_2^2 - \omega^2 + i\omega\gamma_2) + k_{34}}{\left[\omega_3^2 - \omega^2 + i\omega\gamma_3 - k_{13}^2/(\omega_1^2 - \omega^2 + i\omega\gamma_1) - k_{23}^2/(\omega_2^2 - \omega^2 + i\omega\gamma_2)\right](\omega_4^2 - \omega^2 + i\omega\gamma_4) - k_{34}^2} F \right|. \tag{4}$$

Because the radiation of the bright mode exhibits an asymmetry line-shape, it can be described by $|c|+|d|$ corresponding to additive reflectance peaks. It is coupled to oscillator 1 and oscillator 2 in turn, leading to the coexistence of double Fano interferences. Fig. 4(b) shows that the calculated result is in excellent agreement with that of our FDTD simulation. The parameters are chosen as $\omega_1 = 1.1$ eV, $\omega_2 = 1.63$ eV, $\omega_3 = 1.62$ eV, $\omega_4 = 1.93$ eV, $k_{13} = 0.05$, $k_{23} = 0.16$, $k_{34} = 0.1$, $\gamma_1 = 0.001$, $\gamma_2 = 0.001$, $\gamma_3 = 0.27$, $\gamma_4 = 0.17$ and $F = 0.25$.

The Mode1 can be viewed as the oscillator 2 couples to the oscillator 3 with the opposing phase [16], giving rise to the EIT-like destructive interference between the subradiant mode and the superradiant mode. Similar to the EIT-like effect, this Fano interference with a low non-zero frequency-detuning results in a less noticeable change of Lorentz line-shape [33], which exhibits small asymmetric dip within the broad peak. And the Mode2 is an original Fano resonance produced by the coupling of narrow and broad spectral lines. It arises from the weakly damped oscillator 1 couples to the strongly damped oscillator 3 that plays the role of a continuum. The distinction with the Mode1 is that the interaction between two oscillators results in constructive and destructive interference phenomena located very close to each other, corresponding to a sharp change between a maximum and a minimum [35]. As can be seen from Fig. 2(a), the damping coefficient of oscillator 1 and oscillator 2 can be decreased in the MIMI structure.

3.3 Effects of Geometric Sizes and Dielectric Environment

Like other conventional plasmonic lattice arrays, we find that the rectangular MIMI blocks arrays can also be tuned by changing the geometric parameters and the refractive index (n_2) of the dielectric environment. Fig. 5(a) shows the two resonant wavelengths are both red-shifted, especially it mostly changes in the Mode2 as the length (a) increases from 210 nm to 250 nm. Because the longer length of rectangular metal blocks can weaken the strength of the in-plane dipoles to restrict fields, the interference intensity of the Mode2 becomes weaker, and the bright mode is enhanced. Fig. 5(b) shows the reflectance dip of Mode1 is red-shifted, whereas the Mode2 is almost unchanged as the height (h) of the rectangular blocks increases from 160 nm to 200 nm. The resonant wavelength and the interferential line-shape of the Mode1 are more sensitive to changes in height. It's like the principle of exciting out-of-plane lattice plasmon (OLP) because the height of metal nanoparticles is a critical parameter to affect the strength of the out-plane quardrupolars [5]. Fig. 5(c) and (d) respectively show the reflectance spectra are tuned by the width (w_2) increasing from 30 nm to 70 nm, and the width (d_1) rising from 30 nm to 70 nm. Both two resonant wavelengths are blue-shifted, and their dips in the Mode1 first deepen and then shallow. The increasing w_2 harms the strength of in-plane dipoles and out-plane quardrupolars, and two Fano interferences gradually fade away when it's higher than 80 nm. Similarly, as the d_1 increases, the quality factor of the dip in Mode1 becomes lower. This is because the coupling strength of anti-phased quardrupolars is weakened by a more extensive distance between two opposing rectangular metal blocks. However, when d_1 increases, the resonance of Mode2 becomes more robust, it can be interpreted as the more asymmetric distribution of rectangular insulator blocks
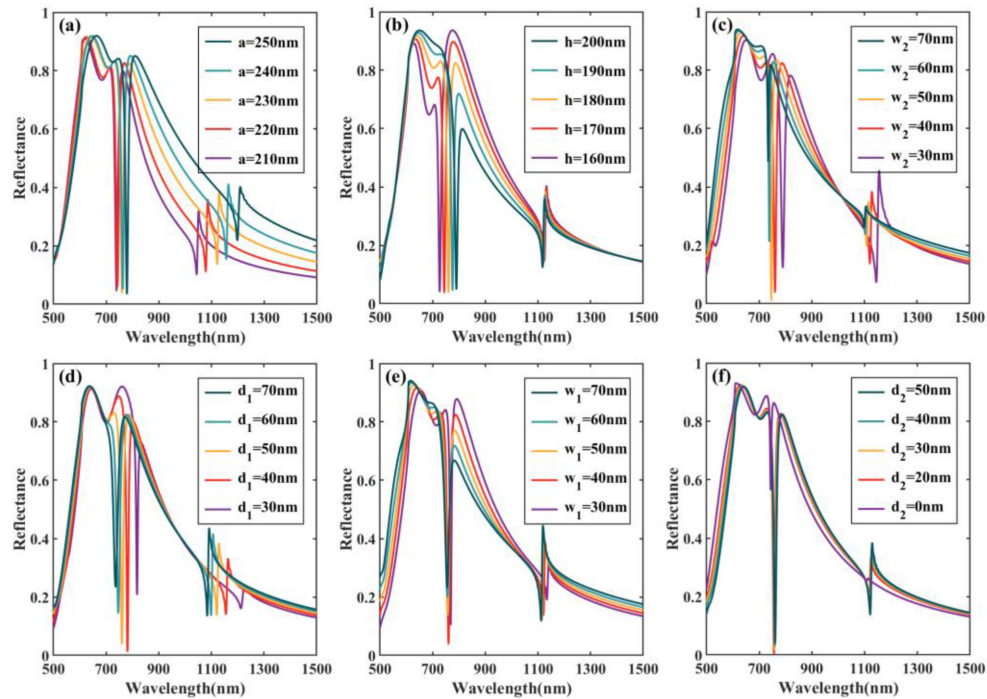
Fig. 5. Reflectance spectra as a function of geometric parameters: (a) a, (b) h, (c) w_2, (d) d_1, (e) w_1, and (f) d_2.
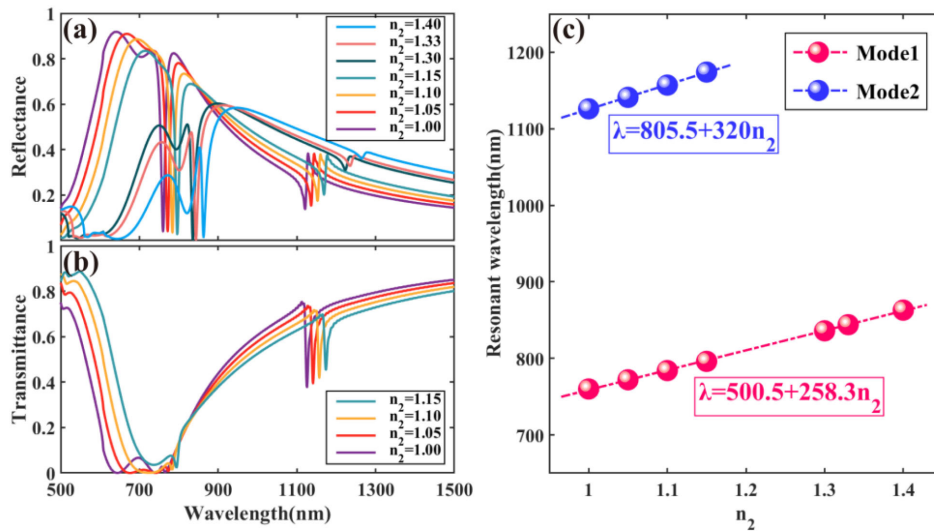

Fig. 6. (a) Reflectance spectra, (b) transmittance spectra, and (c) resonant wavelengths as a function of n_2 in different dielectric environments.

can enhance the difference of damping rates between oscillator 1 and oscillator 3. This interesting phenomenon can also be observed when the width (d_2) increases from 0 nm to 50 nm in Fig. 5(f). When d_2 is wider than 30 nm, the increasing width (d_2) hardly affects Mode1. Fig. 5(e) shows the reflectance spectra are tuned by the width (w_1) increases from 30 nm to 70 nm. The two resonant wavelengths are both blue-shifted when the w_1 increases. And the differences with w_2 are that the

increasing w_1 enhances the resonance strength of the Mode2 and reduces the quality factor of the Mode1.

Finally, we simulate the reflectance and the transmittance spectra by changing the superstrate refractive index (n_2). As shown in Fig. 6(a) and (b), given the substrate with $n_1 = 1.52$, obvious red-shifts of two resonant wavelengths are observed as n_2 increases. When the dielectric environment becomes more symmetric, two reflectance peaks forming the bright mode gradually overlap. However, as n_2 is higher than 1.3, the Mode1 continuously exhibits Fano line-shape with the separation of two reflectance peaks, and Mode2 also fades away. We further show these red-shifts scales linearly with n_2 in Fig. 6(c). The sensitive changes of the reflectance dip in the Mode1 and the transmittance dip in Mode2 following with dielectric environment can be applied in many sensing fields. The bulk index sensitivities (defined as $S = d\lambda/dn_2$) of 258.3 nm/RIU and 320 nm/RIU are achieved by linear fitting for the Mode1 and the Mode2, respectively. For practical applications, the FOM (defined as FOM $= S/\Delta\lambda$) of a sensor is another important parameter to evaluate their performance. The FOM of our plasmonic lattice arrays can reach as high as 20.6 for the Mode1 utilized in Opto-microfluid sensing ($n_2 \sim 1.33$), 28.7 and 38.6 for the Mode1 and the Mode2 used in gas sensing ($n_2 \sim 1.0$), respectively.

4. Conclusion

In conclusion, we have theoretically demonstrated that double Fano interference can be observed in metal-insulator block arrays. The calculative linear-optical spectra reveal a clear manifestation of double Fano resonances. Although the typical experimental results show more losses than that predicted by the Johnson and Christy data, more importantly, we provide a new method to analyze different Fano interferences and strategy to excite dark modes. Under a normal incident, the arrays generate two different extreme field enhancement within the middle insulator, resulting in the absorbance spectrum exhibits two peaks with high-quality factors of 84.92 and 214.1 at wavelengths of 760 nm and 1124 nm respectively. We have observed that the double Fano resonance can be spectrally tuned by a systematic size variation of the metal-insulator block arrays. Our FDTD simulated spectra are in good qualitative agreement with theoretical results obtained by using the coupled harmonic oscillators approximation. Also, we have shown the arrays can be tuned by changing the geometric parameters and dielectric environment. The highly sensitive changes of resonant wavelengths in different n_2 and the FOM have a promising application in biological sensing.

Disclosures

The authors declare no conflicts of interest.

References

[1] L. Novotny and B. Hecht, *Principles of Nano-Optics*. Cambridge, MA, USA: Cambridge Univ. Press, 2012.
[2] B. B. Rajeeva, L. Lin, and Y. Zheng, "Design and applications of lattice plasmon resonances," *Nano Res.*, vol. 11, pp. 4423–4440, Aug. 2018.
[3] W. Wang, M. Ramezani, A. I. Väkeväinen, P. Törmä, J. G. Rivas, and T. W. Odom, "The rich photonic world of plasmonic nanoparticle arrays," *Mater. Today*, vol. 21, no. 3, pp. 303–314, Apr. 2018.
[4] V. G. Kravets, A. V. Kabashin, W. L. Barnes, and A. N. Grigorenko, "Plasmonic surface lattice resonances: A review of properties and applications," *Chem. Rev.*, vol. 118, no. 12, pp. 5912–5951, Jun. 2018.
[5] G. Han, Y. Li, and G. Li, "Necessary conditions for out-of-plane lattice plasmons in nanoparticle arrays," *J. Opt. Soc. Am. B*, vol. 36, no. 4, pp. 805–810, Jan. 2019.
[6] W. Zhou and T. W. Odom, "Tunable subradiant lattice plasmons by out-of-plane dipolar interactions," *Nat. Nanotechnol.*, vol. 6, pp. 423–427, May 2011.
[7] M. Rahmani, B. Luk'yanchuk, and M. Hong, "Fano resonance in novel plasmonic nanostructures," *Laser Photon. Rev.*, vol. 7, no. 3, pp. 329–349, Jul. 2013.
[8] B. Luk'yanchuk *et al.*, "The fano resonance in plasmonic nanostructures and metamaterials," *Nat. Mater.*, vol. 9, pp. 707–715, Aug. 2010.

[9] P. Fan, Z. Yu, S. Fan, and M. L. Brongersma, "Optical fano resonance of an individual semiconductor nanostructure," *Nat. Mater.*, vol. 13, pp. 471–475, Apr. 2014.

[10] N. Liu *et al.*, "Plasmonic analogue of electromagnetically induced transparency at the drude damping limit," *Nat. Mater.*, vol. 8, pp. 758–762, Jul. 2009.

[11] C.-Y. Chen, I.-W. Un, N.-H. Tai, and T.-J. Yen, "Asymmetric coupling between subradiant and superradiant plasmonic resonances and its enhanced sensing performance," *Opt. Exp.*, vol. 17, no. 17, pp. 15372–15380, Aug. 2009.

[12] D.-J. Cai *et al.*, "Fano resonances generated in a single dielectric homogeneous nanoparticle with high structural symmetry," *J. Phys. Chem. C*, vol. 119, no. 8, pp. 4252–4260, Feb. 2015.

[13] N. I. Zheludev, S. L. Prosvirnin, N. Papasimakis, and V. A. Fedotovet, "Lasing spaser," *Nat. Photon.*, vol. 2, pp. 351–354, May 2008.

[14] W.-S. Chang *et al.*, "A plasmonic fano switch," *Nano Lett.*, vol. 12, no. 9, pp. 4977–4982, Aug. 2012.

[15] C. W. Hsu *et al.*, "Observation of trapped light within the radiation continuum," *Nature*, vol. 499, pp. 188–191, Jul. 2013.

[16] M. F. Limonov, M. V. Rybin, A. N. Poddubny, and Y. S. Kivshar, "Fano resonances in photonics," *Nat. Photon.*, vol. 11, pp. 543–554, Sep. 2017.

[17] B. Gallinet and O. J. F. Martin, "Influence of electromagnetic interactions on the line shape of plasmonic fano resonances," *ACS Nano*, vol. 5, no. 11, pp. 8999–9008, Oct. 2011.

[18] M. J. Huttunen, K. Dolgaleva, P. Törmä, and R. W. Boyd, "Ultra-strong polarization dependence of surface lattice resonances with out-of-plane plasmon oscillations," *Opt. Exp.*, vol. 24, no. 25, pp. 28279–28289, Nov. 2016.

[19] X. Yang, G. Xiao, Y. Lu, and G. Li, "Narrow plasmonic surface lattice resonances with preference to asymmetric dielectric environment," *Opt. Exp.*, vol. 27, no. 18, pp. 25384–25394, Aug. 2019.

[20] S. Zou, N. Janel, and G. C. Schatz, "Silver nanoparticle array structures that produce remarkably narrow plasmon lineshapes," *J. Chem. Phys.*, vol. 120, 2004, Art. no. 10871.

[21] M. Hentschel, M. Saliba, R. Vogelgesang, H. Giessen, A. P. Alivisatos, and N. Liu, "Transition from isolated to collective modes in plasmonic oligomers," *Nano Lett.*, vol. 10, no. 7, pp. 2721–2726, Jun. 2010.

[22] J. A. Fan *et al.*, "Fano-like interference in self-assembled plasmonic quadrumer clusters," *Nano Lett.*, vol. 10, no. 11, pp. 4680–4685, Feb. 2010.

[23] M. Hentschel, D. Dregely, R. Vogelgesang, H. Giessen, and N. Liu, "Plasmonic oligomers: The role of individual particles in collective behavior," *ACS Nano*, vol. 5, no. 3, pp. 2042–2050, Feb. 2011.

[24] N. Wang, M. Zeisberger, U. Huebner, V. Giannini, and M. A. Schmidt, "Symmetry-breaking induced magnetic fano resonances in densely packed arrays of symmetric nanotrimers," *Sci Rep*, vol. 9, 2019, Art. no. 2873.

[25] C.-Y. Huang and H. Chang, "Plasmon coupling within the multifold nanorod metasurface for sensing applications," *IEEE Photon. J.*, vol. 11, no. 1, Feb. 2019, Art. no. 4800208.

[26] W. Zhao, X. Leng, and Y. Jiang, "Fano resonance in all-dielectric binary nanodisk array realizing optical filter with efficient linewidth tuning," *Opt. Exp.*, vol. 23, no. 5, pp. 6858–6866, Mar. 2015.

[27] F. Hao, Y. Sonnefraud, P. V. Dorpe, S. A. Maier, N. J. Halas, and P. Nordlander, "Symmetry breaking in plasmonic nanocavities: Subradiant LSPR sensing and a tunable fano resonance," *Nano Lett*, vol. 8, no. 11, pp. 3983–3988, Oct. 2008.

[28] V. A. Fedotov, M. Rose, S. L. Prosvirnin, N. Papasimakis, and N. I. Zheludev, "Sharp trapped-mode resonances in planar metamaterials with a broken structural symmetry," *Phys. Rev. Lett.*, vol. 99, 2007, Art. no. 147401.

[29] K. Jiang, M. Lu, S. K. Gupta, and Y. Chen, "A trapped mode by higher-order Fano-like interference in a symmetric plasmonic structure," *Appl. Phys. A*, vol. 123, 2017, Art. no. 676.

[30] Y. S. Joe, A. M. Satanin, and C. S. Kim, "Classical analogy of fano resonances," *Phys. Script.*, vol. 74, pp. 259–266, Jul. 2006.

[31] P. B. Johnson and R. W. Christy, "Optical constants of the noble metals," *Phys. Rev. B*, vol. 6, pp. 4370–4379, Dec. 1972.

[32] E. D. Palik, *Handbook of Optical Constants of Solids*. New York, NY, USA: Academic Press, 1998.

[33] B. Peng, Ş. K. Özdemir, W. Chen, F. Nori, and L. Yang, "What is and what is not electromagnetically induced transparency in whispering-gallery microcavities," *Nat Commun.*, vol. 5, 2014, Art. no. 5082.

[34] A. B. Evlyukhin, C. Reinhardt, A. Seidel, B. S. Luk'yanchuk, and B. N. Chichkov, "Optical response features of Si-nanoparticle arrays," *Phys. Rev. B*, vol. 82, no. 4, 2010, Art. no. 045404.

[35] A. E. Miroshnichenko, S. Flach, and Y. S. Kivshar, "Fano resonances in nanoscale structures," *Rev. Mod. Phys.*, vol. 82, pp. 2257–2298, Aug. 2010.